Structural Safety 121 (2026) 102717

Contents lists available at ScienceDirect

Structural Safety

journal homepage: www.elsevier.com/locate/strusafe

Evaluation of the safety ratio in the Eurocode for deck acceleration limit on ballasted railway bridges

Gonçalo Ferreira [a,*], Pedro Montenegro [a], Christoph Adam [b], António Abel Henriques [c], Rui Calçada [a]

[a] CONSTRUCT-iRAIL - Faculty of Engineering, University of Porto, Rua Dr. Roberto Frias, 4200-465, Porto, Portugal
[b] Universität Innsbruck, Unit of Applied Mechanics, Technikerstr. 13, 6020 Innsbruck, Austria
[c] CONSTRUCT-LABEST - Faculty of Engineering, University of Porto, Rua Dr. Roberto Frias, 4200-465, Porto, Portugal

ARTICLE INFO

Keywords:
Ballasted railway bridge
Eurocode
Deck acceleration
Safety ratio
Subset simulation

ABSTRACT

Ballasted railway bridges are subject to dynamic excitation from passing trains, which can cause excessive vibrations in the ballast bed depending on the train speed, resulting in track instability. The Eurocode EN 1990 uses vertical deck acceleration as an indicator of safety, limited it to 3.5 m/s^2 for ballasted bridges. Since experimental studies show that ballast instability occurs at about 7.0 m/s^2, the normative limit seems to be arbitrarily based on a safety ratio of 2.0. The present paper examines the suitability of a lower safety ratio. The proposed methodology compares the physical acceleration limit with the design acceleration calculated at a critical speed corresponding to a failure probability of 10^{-4}. An algorithm for the efficient assessment of critical speeds based on subset simulation is introduced, together with a parametric study for its optimization. A sensitivity analysis of the random variables of ballasted bridges allows the definition of two design scenarios in accordance with the Eurocode EN 1991-2. Results from the application of the methodology to four case study bridges show that design accelerations greater than the limit defined in the Eurocode can be found in ballasted bridges within the target probability of failure, suggesting that the safety ratio may be set lower than 2.0.

1. Introduction

1.1. Normative context and physical bias

In the Eurocode EN 1990 [1], vertical deck acceleration is the limit criterion adopted for ballasted railway bridges, with a limit of 3.5 m/s^2 for vertical deck acceleration. The corresponding traffic actions are prescribed in the EN 1991-2 [2] through the High-Speed Load Model (HSLM), which provides envelope train configurations for design and verification. Historically, this 3.5 m/s^2 threshold traces back to test campaigns that reported the occurrence of ballast instability at approximately 0.7 g ≈ 7.0 m/s^2, as documented in reports by the European Rail Research Institute and subsequent replications [3,4]. The halving of the observed instability level to define the current limit implies that a safety ratio of 2.0 was employed for the EN 1990, yet the basis for this value has been questioned [4]. More recently, the European Union Agency for Railways (ERA) [5] highlighted the need to the revisit acceleration limits as part of closing open points in the bridge dynamics domain of the Technical Specification for Interoperability [6].

While the 3.5 m/s^2 limit is entrenched in current practice, the normative safety ratio that it is based on has not been rigorously established against probabilistic targets or variability in bridge/track parameters. This motivates re-examining whether a lower ratio could still meet a commonly accepted target reliability.

1.2. Ballast behavior and track stability

Railway bridges with ballasted track systems undergo complex dynamic behavior in which ballast stiffness, deck mass/stiffness, damping, and support conditions jointly shape acceleration responses. Recent work using laboratory rigs and system identification has clarified the limited contribution of ballast stiffness to bending frequencies for short spans, emphasizing the need to model the system holistically [7,8]. Regarding track stability, studies indicate that momentary peaks may not immediately cause instability [8], whereas cumulative vibration occurrence can become relevant, suggesting an analogy with fatigue-like damage accumulation [9]. Mitigation strategies such as ballast mats have been assessed experimentally and numerically for vibration control, including on bridges [10]. For modeling the vertical ballast response in simulations, widely used formulations remain a

* Corresponding author.
E-mail address: gcferreira@fe.up.pt (G. Ferreira).

https://doi.org/10.1016/j.strusafe.2026.102717
Received 23 March 2025; Received in revised form 13 February 2026; Accepted 5 April 2026
Available online 24 April 2026

practical basis when combined with calibrated damping and support models [11].

Existing research clarifies the mechanisms involved and practical mitigation techniques, but does not translate these insights into deterministic design scenarios aligned with the EN 1991-2's guidance on stiffness/damping/mass bounds to compute deck accelerations at speeds that are probabilistically critical. This realization leads to the development of explicit, implementable scenarios that structural engineers can use during design checks.

1.3. Reliability and probabilistic approaches for railway bridges

Probabilistic studies on structures are characterized by both aleatory and epistemic uncertainties. The former can be categorized into three types [12]: uncertainties in excitation (differences in operating trains, vehicle properties, running speed, or rail irregularities), structural variability (material properties, structural damping, construction methods, ballast models, or subsoil characteristics), and impact from the environment (temperature, humidity, sediments, or deterioration). The probabilistic study in this work focuses on aleatory uncertainties in material properties, geometry, damping, supports, and track parameters, modeled as random variables based on observed variability [11,13]. Epistemic uncertainty, such as model-form error (e.g., beam vs. 3D FE representation), is acknowledged but not explicitly treated in the present study. Previous studies [13–16] show that response distributions vary with depending on proximity to resonance, being approximately normal when far from it, but skewed and heavy-tailed otherwise. Sensitivity analyses confirm that mass, stiffness, and damping dominate variability, while track irregularities and environmental effects can significantly influence resonance behavior. The influence of individual uncertainties on the acceleration response is highly speed-dependent [14]. These considerations support the selection of basic random variables and the probabilistic framework adopted in this study. A detailed discussion of these uncertainty sources and their treatment can be found in Salcher et al. [12].

Since deck accelerations are affected by parameter uncertainty and operational variability, train-bridge dynamics has increasingly been addressed with probabilistic methods. Alternatives to crude Monte Carlo such as the Probability Density Evolution Method and Response Surface Model [15–18] have been used to propagate uncertainty efficiently, highlighting influential parameters in coupled models and risk assessment. For reliability assessment at low probabilities of failure relevant to either serviceability or running safety, studies have employed tail modeling, FORM, line sampling, and subset simulation to reduce computational cost while maintaining accuracy [14,19–24]. Target reliability levels around $\beta \approx 3.7\,(p_f \approx 10^{-4})$, recommended by the Joint Committee on Structural Safety considering Class 3 consequences with high cost of safety measures, provide a usable benchmark for bridge safety checks [25]. At such low probabilities of failure, crude Monte Carlo becomes prohibitive (requiring samples sizes $N \approx 10^4$ to 10^5 for stable estimates [26]), whereas subset simulation achieves the same order efficiently by decomposing rare events into a sequence of intermediate conditional events [27,28].

Prior work demonstrates the tools (subset simulation and related techniques) and the targets $(p_f \approx 10^{-4})$, but no study has closed the loop to reassess the Eurocode deck acceleration limit (and its implied safety ratio) by locating critical speeds at which the probability of failure crosses the target, and consequently mapping those probabilistic results onto deterministic design scenarios.

1.4. Research gaps and contributions of the study

In light of the presented considerations, the following needs are addressed:

1. *Critical speeds at low probabilities of failure.* Critical speed is defined for the HSLM trains as the lowest speed at which $p_f \geq 10^{-4}$. An efficient search algorithm that leverages subset simulation is developed to locate this speed without exhaustive sampling across the speed range.
2. *Design scenarios consistent with the EN 1991-2.* Two deterministic scenarios that implement EN 1991-2's guidance on lower bound estimates of stiffness/damping and both lower and upper bounds of mass are derived by selecting the most influential variables via a targeted sensitivity study, enabling practical calculation of design accelerations.
3. *Reassessment of the safety ratio.* By comparing the design acceleration at the probabilistic critical speed to the physical instability threshold of 7.0 m/s^2 (observed from experimental evidence) it is evaluated whether the implied safety ratio of 2.0 is conservative and whether lower ratios can still meet $p_f \approx 10^{-4}$.

To address these issues, the present article proposes definitions for a safety ratio, design scenarios, and critical speed in Section 2, followed by the introduction of an algorithm for their efficient assessment in Section 3. Four case study bridges are presented in Section 4. A parametric study to optimize the critical speed algorithm is given in Section 5, allowing the calculation of critical speeds in Section 6. In the same Section, after a sensitivity analysis of the random variables, two design scenarios are proposed, and the final safety ratios are calculated. The conclusions in Section 7 summarize findings and outline directions for future research.

2. Methodology

2.1. Physical problem

The physical problem addressed in this study is the dynamic response of ballasted track railway bridges subject to high-speed train loading. Under excessive deck accelerations, the interlocking capability of the ballast particles can become compromised, leading to a loss of resistance in the load path from the rails to rail pads, sleepers, and ballast bed. Such issues require track maintenance, which can mean an interruption of train service, with a significant impact on rail operations. Ultimately, an unmaintained ballast track can be the cause of derailment. In ballasted bridges, this limit state is here considered to occur when vertical deck acceleration exceeds 7.0 m/s^2.

2.2. Bridge modeling and deterministic formulation

The presented physical problem is studied on bridge models, with the purpose of determining the underlying safety ratios. All bridges studied are represented by finite element models, constructed by employ the modeling technique developed by Rocha [13], adapted for the ANSYS® [29] environment. In this technique, the ballast layer, rail pads, and supports are modeled with spring-dashpot elements (COMBIN14), while the rails and deck are discretized with beam elements (BEAM3). The localized masses of the sleepers are represented by mass elements (MASS21). Fig. 1 illustrates the typical FE model implementation adopted in this work.

In probabilistic analyses, used for the estimation of critical speed, the models' material and geometrical properties are defined with random variables, detailed in Section 4. In deterministic analyses, used in the design phase, the models are used to compute deck accelerations under the High-Speed Load Model defined in the EN 1991-2 [2], considering the same norm's provisions for stiffness, mass, and damping conditions. These models form the basis for the design scenarios introduced later in this section.

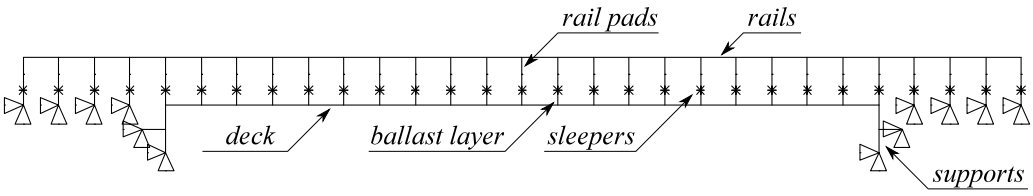

Fig. 1. Finite element model.

2.3. Estimation of safety ratios

The procedure for calculating safety ratios for existing bridges is described in the present section, along with the necessary definitions. It is divided into three steps, which are outlined in Fig. 2 and developed in the following subsections. The first step (Section 2.3.1) is to determine the speed at which a load model causes an excessive deck acceleration. This first step involves probabilistic analysis using bridge models constructed with random variables. After finding the critical speed (v_{crit}), the second step (Section 2.3.2) is to determine the acceleration value that can be calculated with fixed values for the variables (instead of probabilistic analysis). The instructions for setting the variables to perform a deterministic analysis are referred to as the design scenarios. Employing such scenarios is beneficial to ensure that trustworthy results are attainable in the engineering practice of bridge design with simple analyses. The third step (Section 2.3.3) is to locate in the design scenarios the acceleration value at the critical speed, here called "design acceleration" (a_{Ed}). The margin between this value and the experimentally assessed limit of 7.0 m/s^2 (a_{Rl}) indicates the distance to safety. Therefore, the safety ratio (γ_{bt}) can finally be estimated by dividing 7 by the design acceleration.

2.3.1. Step 1: Find the critical speed

This study of ballasted track bridges assesses failure due to track instability (loss of stability of the ballast layer), assuming that the 7.0 m/s^2 value for vertical deck acceleration is the value experimentally deemed to cause failure that acts as the safety threshold. Therefore, a failure event is considered to have occurred if a bridge deck experiences a vertical acceleration a greater than this limit (a_{Rl}) when subjected to any load model, at any given train speed. It is also assumed that the loss of stability can ultimately lead to derailment, and that this risk corresponds to Class 3 consequences as defined in the Probabilistic Model Code of the JCSS [25]. The authors consider that the relative cost of safety measures (extensive measurements through safety inspections over significant periods of time) is large. In the Probabilistic Model Code, this combination of consequence and cost corresponds to a target reliability index β of 3.7, which corresponds to probabilities of failure in the order of magnitude of 10^{-4}. The probability of failure p_f is therefore defined as:

$$p_f = P\left(a \geq a_{Rl}\right) \tag{1}$$

When testing a load model, different train speeds result in different maximum values of vertical deck acceleration. For this study, a critical speed is defined, for a given load model, as the lowest speed that causes the following condition:

$$p_f \geq 10^{-4} \tag{2}$$

The evaluation focuses on the first occurrence of the limit state being surpassed rather than the absolute maximum acceleration, in alignment with reliability-based design principles. The High-Speed Load Model (HSLM-A) [2], whose purpose is to represent the envelope of actions of real high-speed rolling stock traffic, is employed in this work. This load model, which is used for the design of high-speed railway bridges, is given as a set of 10 configurations of axle loads and spacings and is intended for moving load analysis. For a given bridge, critical speeds can be calculated for each of the 10 HSLM-A. These individual critical speeds are here identified as $v_{crit,i}$. The lowest of the individual critical speeds obtained is then taken as the critical speed v_{crit} of the bridge.

2.3.2. Step 2: Determine the design scenarios

The scenarios for bridge design are defined in this study as sets of deterministic values attributed to structural and track variables utilized to calculate the dynamic response of railway bridges. Two sets are defined, in accordance with the provisions of Eurocode EN 1991-2 [2], which requires a lower bound estimate of stiffness and structural damping and both upper and lower bound estimates of mass. This procedure is meant to maximize the acceleration response and to avoid overestimating the resonant speed. In spite of this statement being present in the Eurocode, the standard does not specify which variables are to be considered in the estimates, nor what constitutes upper or lower bounds. This study employs random variables that follow normal or uniform distributions to describe geometrical and material properties of the bridge models, detailed in Section 4. Here, it is proposed to consider as lower and upper bounds estimates the 5th and 95th percentiles, respectively. For random variables that follow normal distributions $N\left(\mu, \sigma^2\right)$, this corresponds to $\mu \pm 1.64\sigma$. Similarly, for uniformly distributed random variables $U\left(a, b\right)$, the lower and upper design bounds correspond to $a + 0.05\left(b - a\right)$ and $a + 0.95\left(b - a\right)$, respectively.

Regarding the selection of random variables to be included in the definition of scenarios, it should be noted that, depending on the complexity of the models employed, stiffness, damping, and mass can be related to more than one variable and even share variables. Therefore, it is necessary to perform a parametric study of the relative influence of each variable. The proposed methodology for such a study starts with setting all variables to their mean value and calculating the resulting deck acceleration envelope considering the 10 HSLM-A. The response vector is $\mathbf{X}$ for a given speed range with k speed values. Then, each variable is independently set to its upper or lower bound, resulting in a new response vector $\mathbf{Y}$ with the same length k. To evaluate the influence of each variable, the variance of the absolute difference between the vectors is calculated as:

$$\mathrm{Var}\left(|\mathbf{X} - \mathbf{Y}|\right) = \frac{\sum_{i=1}^{k}\left(|\mathbf{X}_i - \mathbf{Y}_i| - \mathrm{E}\left(|\mathbf{X}_i - \mathbf{Y}_i|\right)\right)}{n-1} \tag{3}$$

Consequently, the most influential variables are included in the definition of the two design scenarios. Both scenarios use a lower bound on the variables that control stiffness and damping. The first scenario (S1) uses a lower bound estimate of mass, while the second (S2) uses an upper bound. The variables that are not considered influential enough after the parametric study are taken at their mean values. This step of the methodology concludes with the calculation of the response envelope of both scenarios under the effect of the 10 HSLM-A configurations.

2.3.3. Step 3: Locate the design acceleration

At this point, the maximum speed that can be considered safe is already known. The remaining question is how far away the design scenarios are from the actual failure events. The value on the envelope of the design scenarios at v_{crit} is here given the name of design acceleration a_{Ed}. The safety ratio, henceforth referred to as γ_{bt}, is defined in this work as the ratio between the experimentally assessed acceleration

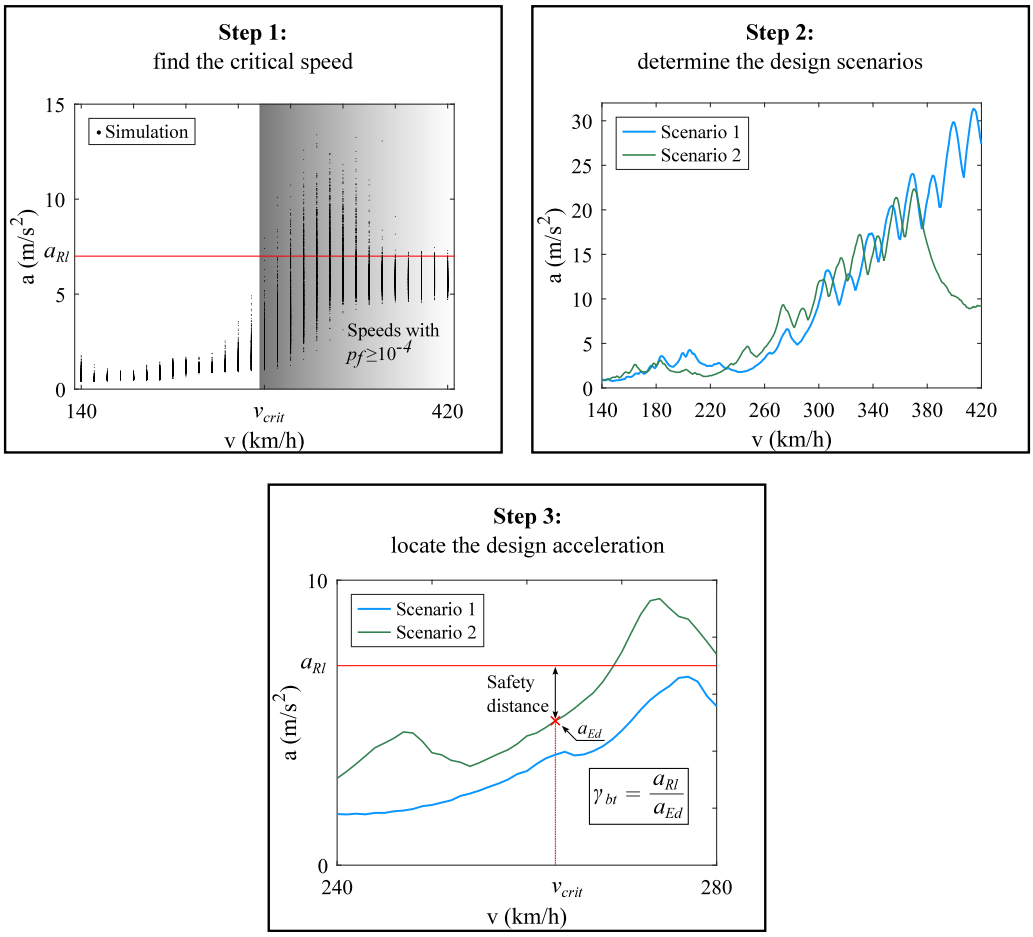

Fig. 2. Overview of the methodology for estimation of safety ratios for the deck acceleration criterion.

limit that causes instability in the ballast layer a_{Rl} and the acceleration calculated in the design phase a_{Ed} and is given by:

$$\gamma_{bt} = \frac{a_{Rl}}{a_{Ed}} = \frac{7}{a_{Ed}} \tag{4}$$

3. Subset simulation application for the estimation of critical speed

3.1. Overview of subset simulation

Monte Carlo simulation, while a highly reliable approach, implies an escalation in computational cost as the intended target probabilities of failure get lower. In fact, according to Bjerager [26], the appropriate sample size N to assess a probability of 10^{-4} would be:

$$\frac{1}{p_f} \leq N \leq \frac{10}{p_f} \Leftrightarrow 10,000 \leq N \leq 100,000 \tag{5}$$

For moving loads analyses (as is the case in the present study) and less complex 2D finite element models, such a number would be feasible. However, any change in the train speed or load model requires a new analysis, and therefore, the search for critical speed can quickly grow to several hundred thousand (or millions) of dynamic analyses.

Therefore, subset simulation (introduced by Au and Beck [27]) is chosen to estimate the probabilities of failure. With this method, p_f is estimated as the conditional probability of reaching the unsafe region in a reliability problem through successive increments of intermediate failure events. The same authors calculate p_f as:

$$p_f = P\left(F_i\right) \prod_{i=1}^{m-1} P\left(F_{i+1} | F_i\right) \tag{6}$$

where F_i are m number of intermediate events (or levels) such that $F_1 \supset F_2 \supset \ldots F_m$. For the first level, $P\left(F_1\right)$ is estimated with a crude Monte Carlo simulation, provided a reasonable N. The resulting values are ordered from highest (belonging to F_1) to lowest (farthest from F_1), as illustrated in Fig. 3(a). Given a selected arbitrary intermediate probability p_0, the $\left(p_0 \times N\right)$-th value is classified as the cut-off y^*. The states of the random variables corresponding to values greater than or equal to y^* are used as generators (x) to generate the sample of the next level $(\tilde{x})$, using the Modified Metropolis Algorithm. This ensures that the states of the variables of the resulting sample are inside F_1. It is visible, in Fig. 3(b), how every result in the second level $(i = 2)$ is greater or equal to the cut-off that defines F_1. The process is repeated (Figs. 3(c) and 3(d)) until y^* is found inside F_m (i.e., $P(F_i) > p_0$).

3.2. Application for railway bridges

Subset simulation is applied in this work to estimate the probability of a bridge deck experiencing vertical accelerations that exceed a given limit, per Eq. (1). The bridges being studied are represented by Finite Element models whose material and geometrical properties follow prescribed random variable distributions. The proposed application begins (for the first subset level $i = 1$) with sampling the random variables (using MATLAB® [30]), and combining them to obtain variations of a basis FE model, which is created in ANSYS® [29].

The dynamic response is calculated for the desired load model (i.e., one of the 10 HSLM-A configurations) using the Single Load Linear Superposition (SLLS) method (introduced by Ferreira et al. [31]), employed due to its efficacy and ease of application. The response is then filtered with a low-pass Type II Chebyshev filter, cut off at 60 Hz. It is

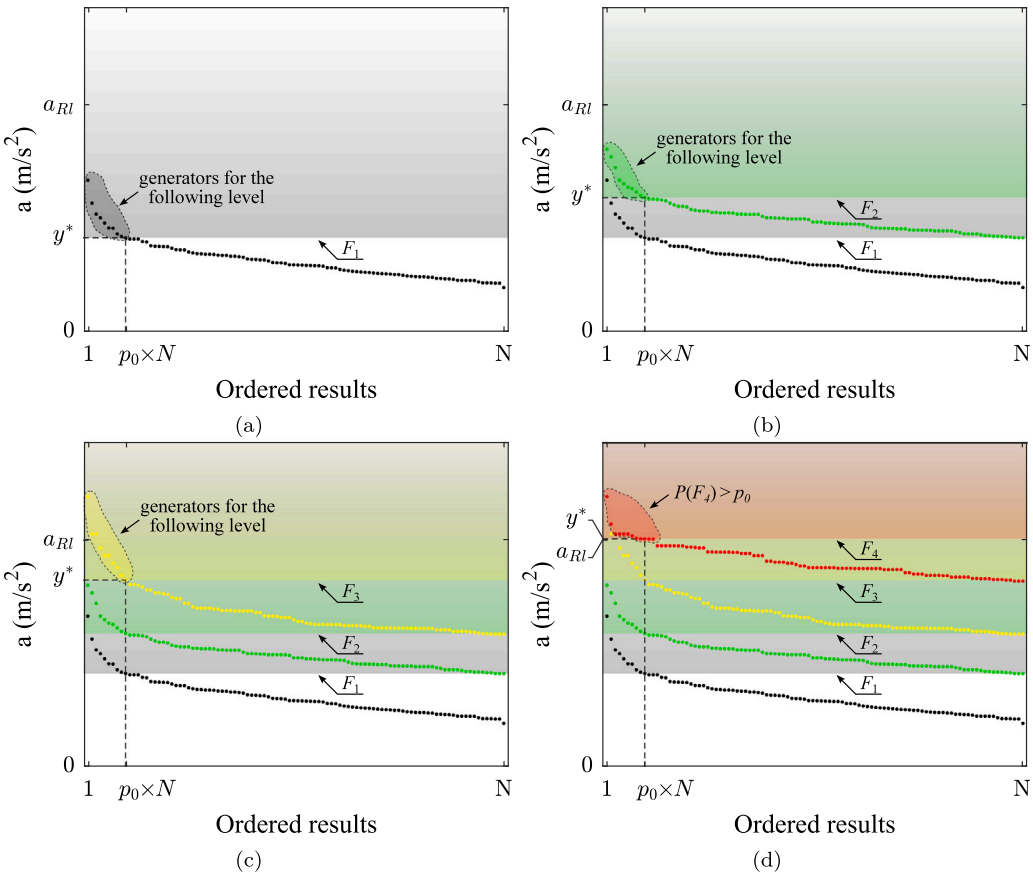

Fig. 3. Visualization of subset simulation. (a) $i = 1$; (b) $i = 2$; (c) $i = 3$; (d) $i = 4$.

worth noting that although the EN 1990 only requires the consideration of frequencies up to 30 Hz, studies have highlighted the importance of extending the frequency range [32]. The maximum absolute value of vertical deck acceleration is stored for each randomly generated bridge.

After this phase, which constitutes a crude Monte Carlo simulation, $P(F_1)$ can be estimated. If it is lower than p_0, the level counter is increased, and the ordered results greater or equal to the cut-off value of y^* are used as the generators (x) in a Markov Chain Monte Carlo (MCMC) process, which produces the sample of the next level $(\tilde{x})$ by employing the Modified Metropolis Algorithm (MMA). For this study, an MMA implementation based on Uribe [33] is used. A key element in applying the MMA is the choice of appropriate proposal Probability Density Functions (PDFs), as noted by Zuev [28]. Proposal PDFs are utilized to obtain candidate states η from a variable's current state x_k. The same author recommends that the proposal PDFs should have spreads that ensure proper acceptance ratios in the MMA. Therefore, in this work, the adopted proposal functions in the case of Gaussian distributed variables are Normal distributions centered at x_k with the same variance of the respective RV:

$$N(\mu, \sigma^2) : \eta \sim N(x_k, \sigma^2) \tag{7}$$

In the case of uniformly distributed variables, the proposal functions are Normal distributions centered at x_k with the variance of the Uniform RV:

$$U(a, b) : \eta \sim N\left(x_k, \frac{(b-a)^2}{12}\right) \tag{8}$$

These functions follow the literature [27,28] to ensure ergodicity and proper acceptance ratios. The η values of all random variables are used in the MMA to produce the following level's sample $(\tilde{x})$, after which new variations of the FE models are obtained, and the dynamic responses for the new set can be calculated. The process stops after the $P(F_i) > p_0$ condition occurs (after which p_f can be estimated) or if $i = m$ (i.e., if the subset simulation process is already in the mth level, any existing p_f would be lower than 10^{-m}, and therefore not worth further exploration for the purposes of this study). The diagram in Fig. 4 illustrates how subset simulation is applied in practice for this study. Its inputs are the basis of FE model, the material and geometry random variables, the load model, and speed range, and its outputs are the maximum vertical deck acceleration per FE model realization and resulting probability of failure. The main steps of the application are:

1. Sample random variables and build FE model variations;
2. Compute the dynamic response for each sample using SLLS;
3. Estimate $P(F_i)$ and determine cut-off y^*;
4. Generate next-level samples via MMA and update the FE models;
5. Repeat until $P(F_i) > p_0$ or the maximum level is reached.

3.3. Critical speed search algorithm

While the previous section detailed how subset simulation can be used to estimate the probability of failure for a given speed, the current section introduces an algorithm that uses these estimates to locate the critical speed efficiently. Although the application of subset simulation is associated with considerable savings in computation time, this only applies to the estimation of probabilities for a given train speed. That is, the question remains for which speed or set of speeds the probabilities must be calculated. Simulating in coarse intervals (e.g. with increments of 10 km/h) is incompatible with the influence that train speed has on the results of dynamic analyses. In fact, such an interval can overlook the existence of a critical speed inside intervals. Conversely, it is not feasible to calculate the probabilities of failure for all values in a usual running speed range with 1 km/h increments.

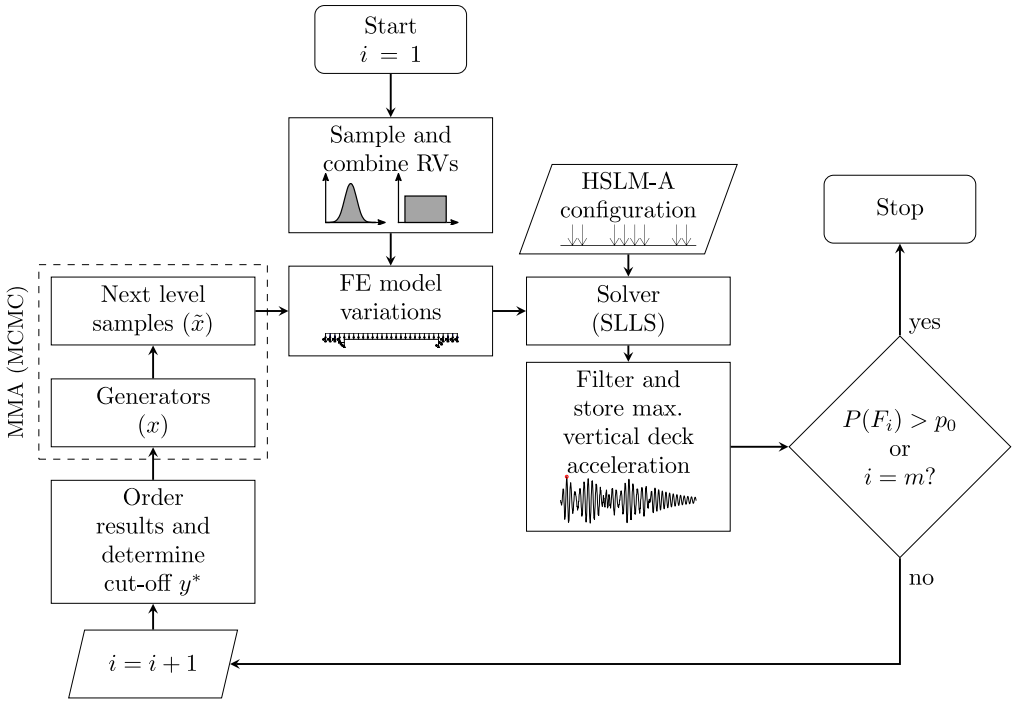

Fig. 4. (Updated) Application of subset simulation for railway bridges.

Hence, an algorithm is proposed here to efficiently assess critical speeds. This procedure looks for a critical speed by firstly doing a coarse search in 20 km/h increments, switching to finer 1 km/h increments only when it considers that a critical speed is likely to be found. This likelihood is assessed for each speed value by evaluating the results of the first level of subset simulation, and comparing them to an appropriately set threshold. If a certain speed value is deemed unlikely to be critical by this criterion, it is discarded. This avoids wasteful use of computational resources, by not calculating probabilities of failure lower than 10^{-5}.

When the search cycle is initialized, the speed v of the load model is set to its starting value (the lowest in the speed range). After the initial analysis (i.e., the crude Monte Carlo simulation in $i = 1$), if the cut-off y^* obtained from the ordered results is lower than a chosen threshold value y_t, the speed is increased to the next value. It is highlighted that y_t must be chosen appropriately so that exceeding it represents a substantial likelihood of that train speed's p_f being in the vicinity of 10^{-4}. The cycle continues until the $y^* > y_t$ condition is satisfied, upon which the subset simulation procedure continues. If the resulting p_f is greater than 10^{-4}, the finer increments running speed cycle is initiated. A logical flag stores the occurrence of this fact. The train speed is brought back to the value immediately after the second-highest calculated speed ($v = v - 19$ km/h), and the search continues, now with finer increments. During this phase, whenever the $y^* > y_t$ condition is not met, another logical flag is activated to store the information that at least one train speed has been discarded during the finer cycle. The cycle continues until the first time that a $p_f > 10^{-4}$ is found. On such an occasion, the current v is classified as a suitable candidate. If no previous speed has been discarded in the finer cycle (i.e., the probabilities of failure caused by the speed values immediately before were calculated because the $y^* > y_t$ condition was met, but turned out to be in the magnitude of 10^{-5} or lower), the candidate is immediately accepted as being v_{crit}. Otherwise, a reverse search cycle is activated (where v is decremented by 1 km/h each cycle) to check the previously discarded speed value until a v_{crit} is confirmed.

The proposed algorithm is summarized in the diagram in Fig. 5, in which F and D represent the logical flags that track, respectively, the initiation of the finer search cycle and the discarding of any speed values due to the $y^* > y_t$ criterion. For this algorithm to be viable in terms of computational savings, it is imperative that the sample size N, intermediate probability p_0, and threshold value y_t parameters are properly set. Unoptimized parameters may lead to inefficient use of simulation capacity for the following reasons:

- Waste of unnecessary time calculating v_{crit} candidates that result in $p_f \approx 0$;
- Increased number of entries in the reverse search cycle;
- Inadequate dispersion in the first level's results, jeopardizing further levels.

Hence, a sensitivity study is performed with the objective of setting appropriate parameters. The metrics adopted are the total computation time required to go from $v = 140$ km/h to v_{crit} and the total sample size n_S required for the simulation. The results are presented in Section 5.

3.4. Example of an algorithm run

A detailed example of a complete run of the proposed algorithm is presently given. The parameters of the algorithm for this example are a sample size per level of $N = 100$, an intermediate probability $p_0 = 0.1$, and a threshold $y_t = 3$ m/s^2. With these values of N and p_0, y^* can be found in each subset simulation level in the $100 \times 0.1 = 10$-th position. The graphics in Fig. 6 depict, for each speed, the distribution of results for each train speed. Different colored dots represent different subset levels. The offset in the dots is meant to improve readability, and does not denote any local change in speed.

In the first seven instances, y^* was found to be lower than y_t, meaning that no subset simulation progresses beyond the first level $i = 1$. In the 8th instance, y^* is greater than y_t, causing the subset simulation to continue, resulting in a calculated p_f of 0.02. This result at 280 km/h causes the finer speed increment cycle to be initiated immediately after 260 km/h, i.e. at 261 km/h. In the instances 9, 10 and 11 (261 km/h, 262 km/h, and 263 km/h, respectively) the y_t criterion is not met. Instance 12, at 264 km/h, meets the criterion and returns $p_f = 5.1 \times 10^{-4}$, making it a suitable v_{crit} candidate. However, since there was at least one discarded speed, the algorithm

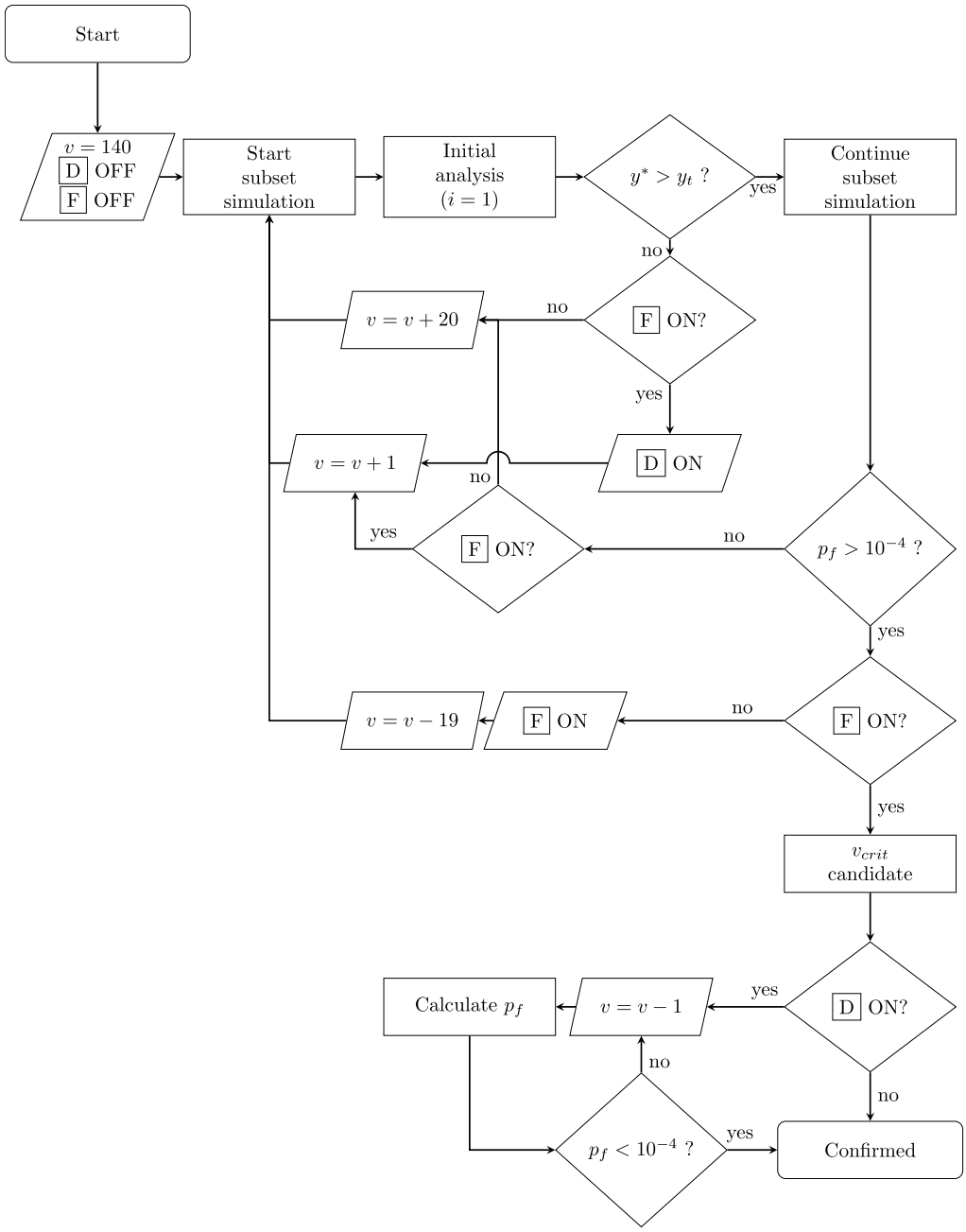

Fig. 5. Algorithm to assess critical speed.

runs instance 13 at 263 km/h. The resulting p_f is 1.2×10^{-4}, making this speed the new v_{crit} candidate. Instance 14, at 262 km/h is also calculated, resulting in $p_f = 4 \times 10^{-5}$, confirming that 263 km/h is v_{crit} and finishing the algorithm run. It is worth noting that this application of the algorithm, with its iterative nature, allowed a critical speed to be found with a total sample size of 2200 (100 per level, with a maximum of 400 per speed value). In contrast, performing a similar procedure using crude Monte Carlo simulations would require a total sample size of over 1 million.

4. Application examples

4.1. Initial considerations

The proposed methodology is applied to four bridges of the Northern Line of the Portuguese Railway Network. The selected set of structures are representative of filler beam bridges, which is a characteristic construction solution of this line. This construction solution consists of simply supported concrete slabs directly cast on embedded steel profiles. Each double-track bridge comprises two independent decks (one for each track), built with directly cast concrete on rolled steel profiles. The track consists of UIC60 rails, wooden sleepers, and a ballast bed. The decks are supported by sets of neoprene bearings located directly under the nine steel profiles on each support.

The choice of modeling technique employed to obtain the bridge responses is supported by two requirements. The first is that the models need to be light enough in order to be used in a subset simulation environment. The other is that they need to describe the main failure mode, which is deck acceleration. Since this metric depends on the vertical response of the deck, and considering that the torsional effects on the sections' eccentricities correspond to high frequencies that are outside the scope of this work (and therefore negligible), the bridge decks can be represented by a single beam model. Additionally, for

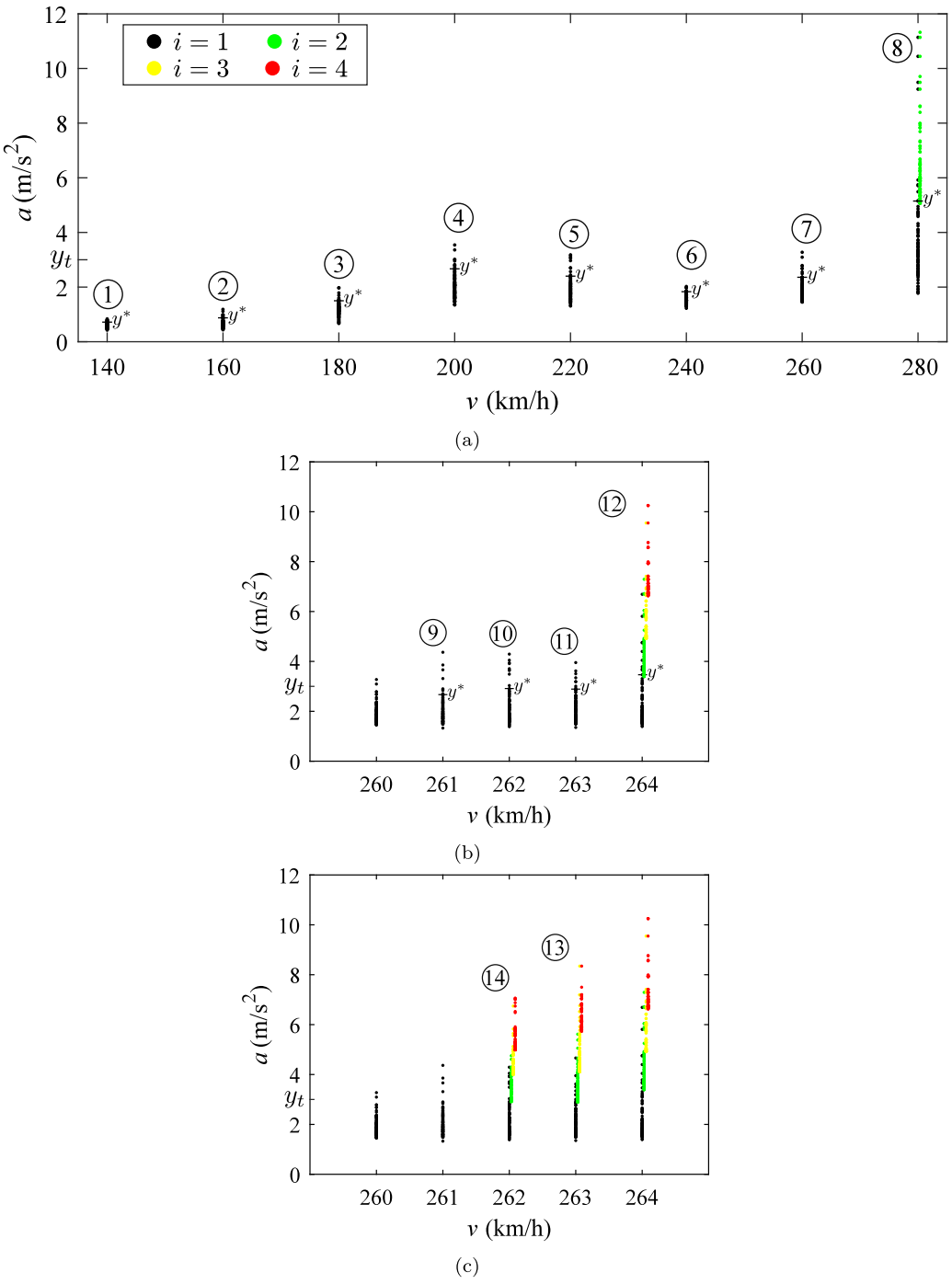

Fig. 6. Example results from the application of the proposed algorithm. (a) Simulations 1 to 8; (b) simulations 9 to 12 (finer speed increment cycle); (c) simulations 13 and 14 ($v = v - 1$ reverse search cycle).

computational efficiency, moving loads analyses are used, and as a consequence, a two-dimensional modeling approach is sufficient to capture the dynamic behavior of the bridges [34,35].

The random variables common to the four models are listed in Table 1, which is adapted from Rocha [13]. As suggested by the author, and supported by Salcher et al. [12], structural random variables are described using Gaussian distributions, since they correspond to material properties with limited dispersion (as the case of the reinforced concrete and structural damping) or controlled geometrical properties (such as the slab's dimensions and the steel profiles' areas). Contrarily, the dispersion that is reported in literature regarding track properties (for the material properties of the ballast, sleepers, rail pads, and track shear stiffness) is more significant [11,36–38]. For this reason, uniform distributions are used to describe the respective random variables.

Each model has three bridge-dependent random variables, which are the thickness (t_{slab}) and width (b_{slab}) of the slab and the area of the steel profiles (A_S). These three variables follow normal distributions, with the mean equal to the nominal value taken from the project drawings and the standard deviation suggested by Rocha [13]. The models also employ quantities taken as constants, which are the steel elasticity modulus E_S (210 GPa), the remaining mass (weight of the waterproofing, guard rails and gutters' box and covers) M_r (1.4 ton/m), the width of the sleeper underside l_b (0.3 m), the half sleeper effective support l_e (0.95 m), the sleeper spacing l_s (0.6 m), and other properties

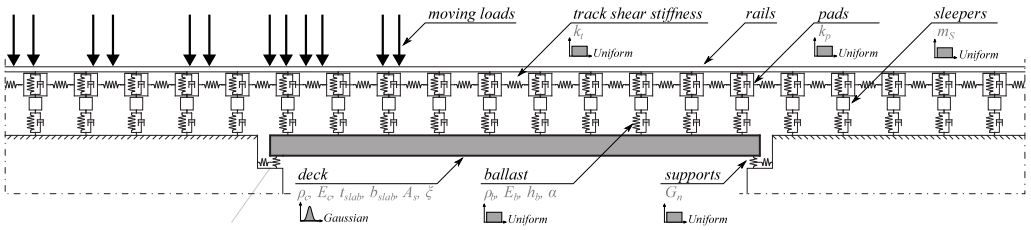

Fig. 7. Schematic representation of the finite element model and random variables.

Table 1
Random variables of the structure, track, and support (adapted from [13]).

Structure variables (Gaussian)	μ	σ
Reinforced concrete density ρ_C	2.5 t/m^3	0.1 t/m^3
Concrete elasticity modulus E_C	36.1 GPa	2.888 GPa
Structural damping ξ	2%	0.3%
Track variables (Uniform)	min.	max.
Ballast density ρ_b	1.5 t/m^3	2.1 t/m^3
Ballast elasticity modulus E_b	80 MPa	160 MPa
Ballast layer height h_b	300 mm	600 mm
Load distribution angle α	15°	35°
Sleeper mass m_s	220 kg	325 kg
Rail pad stiffness k_p	100 kN/mm	600 kN/mm
Track shear stiffness k_t	1×10^4 kN/m/m	3×10^4 kN/m/m
Support variables (Uniform)	min.	max.
Neoprene shear modulus G_n	0.75 MPa	1.5 MPa

of the steel profiles (such as mass $M_{profile}$, moment of inertia $I_{profile}$ and height of the center of gravity $y_{profile}$). The vertical stiffness of the ballast layer is calculated according to Zhai et al. [11], while the supports' vertical and horizontal stiffnesses use the equations given by Manterola [39] and Rocha [13]. Since the methodology utilizes the Single Load Linear Superposition [31] method to calculate the HSLM response, the model only needs to be subjected to a single moving load. The single load's response is calculated with direct integration, using Rayleigh damping matrices (set to the first and second vertical modes of vibration) for the structural damping of the models. A schematic representation of the typical model components is given in Fig. 7.

4.2. Case study bridges

4.2.1. Canelas bridge

The Canelas bridge, consisting of 6 spans, is the only multi-span structure of the set, although the spans are simply supported. Each span has a determinant length of 11.5 m. The cross-section and view of the first span of the Canelas bridge can be seen in Fig. 8. The steel profiles used are HEB500 and the bridge dependent variables for this structure are defined as $t_{slab} \sim N\left(0.7, 0.01^2\right)$ m, $b_{slab} \sim N\left(4.475, 0.005^2\right)$ m and $A_S \sim N\left(0.01975, 0.00079^2\right)$ m^2. As a benchmark, when taking all random variables as their mean values, the first vertical bending mode of the model has a frequency of 8.60 Hz, which is in the vicinity of the 8.70 Hz frequency experimentally assessed by Bonifácio et al. [40].

4.2.2. Melga bridge

With a determinant span length of 23.78 m, the Melga bridge (Fig. 9) is the longest of the set. It consists of a single simply supported span with HEB800 profiles. Both its decks, independent of each other, support a single track. The bridge dependent variables are defined as $t_{slab} \sim N\left(0.871, 0.01^2\right)$ m, $b_{slab} \sim N\left(4.20, 0.005^2\right)$ m and $A_S \sim N\left(0.03342, 0.00079^2\right)$ m^2.

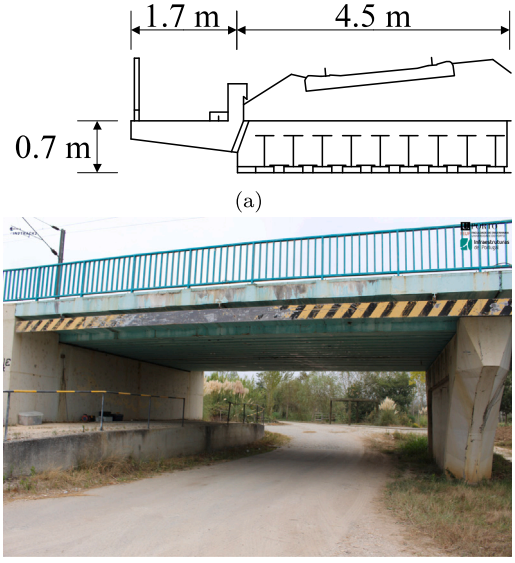

Fig. 8. Canelas bridge. (a) cross-section (unit: m) (adapted from Pimentel et al. [41]); (b) view of the first span.

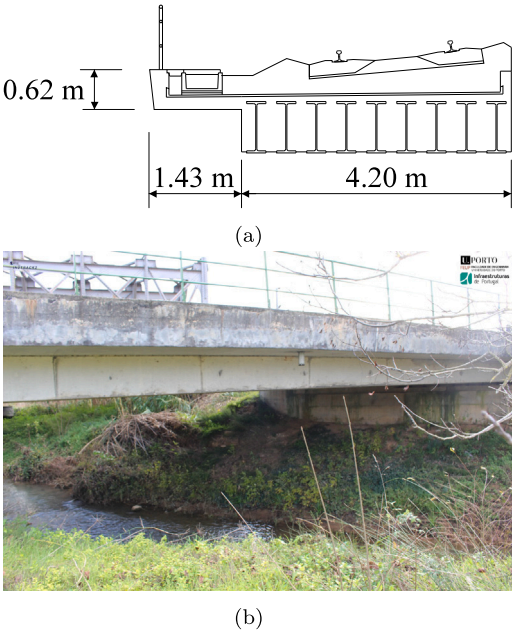

Fig. 9. Melga bridge. (a) cross-section (unit: m); (b) view of the deck.

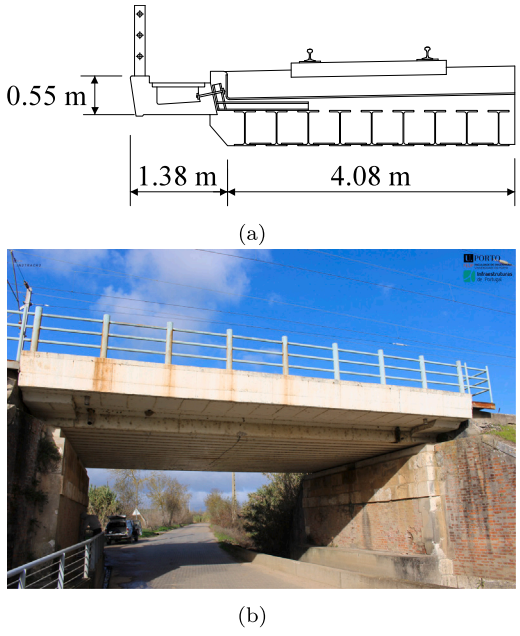

Fig. 10. Cascalheira underpass. (a) cross-section (unit: m); (b) view of the deck.

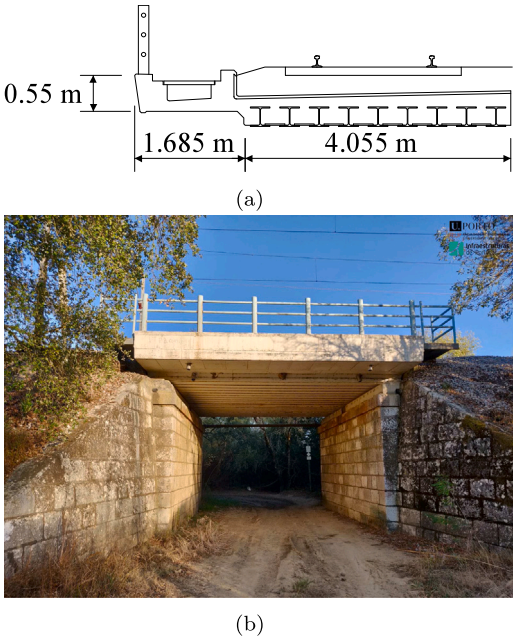

Fig. 11. Braço do Cortiço underpass. (a) cross-section (unit: m); (b) view of the deck.

4.2.3. Cascalheira underpass

The Cascalheira underpass (Fig. 10) consists of a single simply supported span of 10.92 m determinant length, with embedded HEB500 steel profiles. It is composed of two independent decks, each carrying one track. The bridge dependent variables are defined as $t_{slab} \sim N\left(0.703, 0.01^2\right)$ m, $b_{slab} \sim N\left(4.08, 0.005^2\right)$ m and $A_S \sim N\left(0.03342, 0.00079^2\right)$ m^2. For comparison, in a scenario where variables are input with their mean values, the first vertical bending modal frequency of the model is 9.45 Hz, and the experimentally assessed frequency is 9.50 Hz [42].

4.2.4. Braço do Cortiço underpass

With a determinant span length of 7.02 m, the Braço do Cortiço underpass (Fig. 11) is the shortest of the set. This single simply supported span has two independent decks, each with a single track. This deck is embedded with HEB300 profiles and its bridge dependent variables are $t_{slab} \sim N\left(0.445, 0.01^2\right)$ m, $b_{slab} \sim N\left(4.055, 0.005^2\right)$ m and $A_S \sim N\left(0.01491, 0.00079^2\right)$ m^2. Taking average values for all the random variables, the first vertical bending frequency is calculated as 17.86 Hz, while the experimentally assessed frequency is 18.01 Hz [42].

4.3. Dynamic response envelopes

Plots of the dynamic response of the four bridge models are shown in Fig. 12. The solid curves illustrate the response of the models when all random variables are considered at their mean values (**X**), while the areas filled in blue and green indicate the envelopes of the dynamic responses when the most influential variables are set at lower (**Y** lower) or upper (**Y** upper) bounds, respectively. The curves represent the maximum of the 10 HSLM-A load configurations for each train speed value.

5. Optimization of the algorithm for efficient assessment of critical speeds

5.1. Optimization of the threshold value y_t

The Canelas bridge and the HSLM-A3 train were selected to perform the optimization study of the critical speed algorithm. The first parameter to be studied was the threshold value y_t for the initial analysis in $i = 1$, which controls whether a speed value is discarded. For this part of the study, the sample size and the intermediate probability were fixed at $N = 100$ and $p_0 = 0.1$, and y_t varied between 2.0 m/s^2, 2.5 m/s^2, 3.0 m/s^2 and 3.5 m/s^2. Table 2 lists the time and the total sample size needed to complete the algorithm, as well as the resulting v_{crit}. It can be seen that using the values of 3.0 m/s^2 and 3.5 m/s^2 resulted in the least computational expense. However, further analysis of the simulation results revealed that the stricter 3.5 m/s^2 limit caused the algorithm to skip $v = 264$ km/h, which would have produced a suitable p_f and therefore a lower (and valid) v_{crit} candidate. Conversely, while it is true that using lower threshold values prevents prematurely discarding of candidate speeds, this option also leads to increased time expenditure, as additional time is spent calculating candidates that are far from the final one. The threshold value $y_t = 3.0$ m/s^2 is henceforth kept as optimal.

Table 2
Variation of the first level threshold y_t (HSLM-A3, $p_0 = 0.1$, $N = 100$).

y_t	2.0 m/s^2	2.5 m/s^2	3.0 m/s^2	3.5 m/s^2
time (h)	3:34	2:58	1:48	1:37
n_S	4200	3400	2200	2100
v_{crit} (km/h)	266	264	263	267

The results of parametric analyses can be verified by establishing a comparison to crude Monte Carlo simulations with large enough sample sizes. Such simulations were conducted considering the same conditions as the optimization study (i.e., for the Canelas bridge FE model under the HSLM-A3 load configuration) and a sample size $N = 100000$, corresponding to the larger value from Eq. (5). The results are shown in Fig. 13, by illustrating the complementary Cumulative Distribution Function (CDF) of a simulation corresponding to a critical speed to the complementary CDF of its equivalent Monte Carlo simulation. In the figures, the circles highlight the acceleration value at the intermediate level (i.e., that simulation's y^* values), while the asterisk indicates the final calculated p_f. It can be seen that there is a close correspondence for the scenarios with $y_t = 2.5$ m/s^2 and $y_t = 3.0$ m/s^2, where not only is the calculated p_f in the same order of magnitude (of 10^{-4}), but the intermediate levels also follow the trend of the corresponding Monte Carlo simulation.

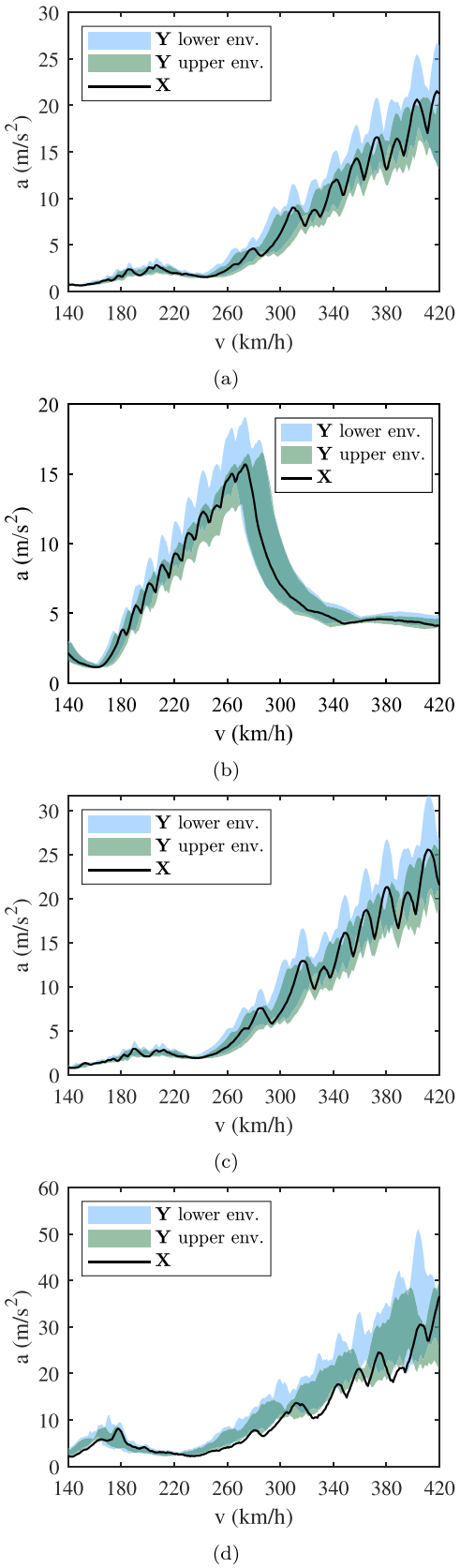

Fig. 12. Dynamic response envelopes considering all random variables with mean values (**X**) and the envelopes of lower and upper bounds of the most influential variables (**Y**). (a) Canelas bridge; (b) Melga bridge; (c) Cascalheira underpass; (d) Braço do Cortiço underpass.

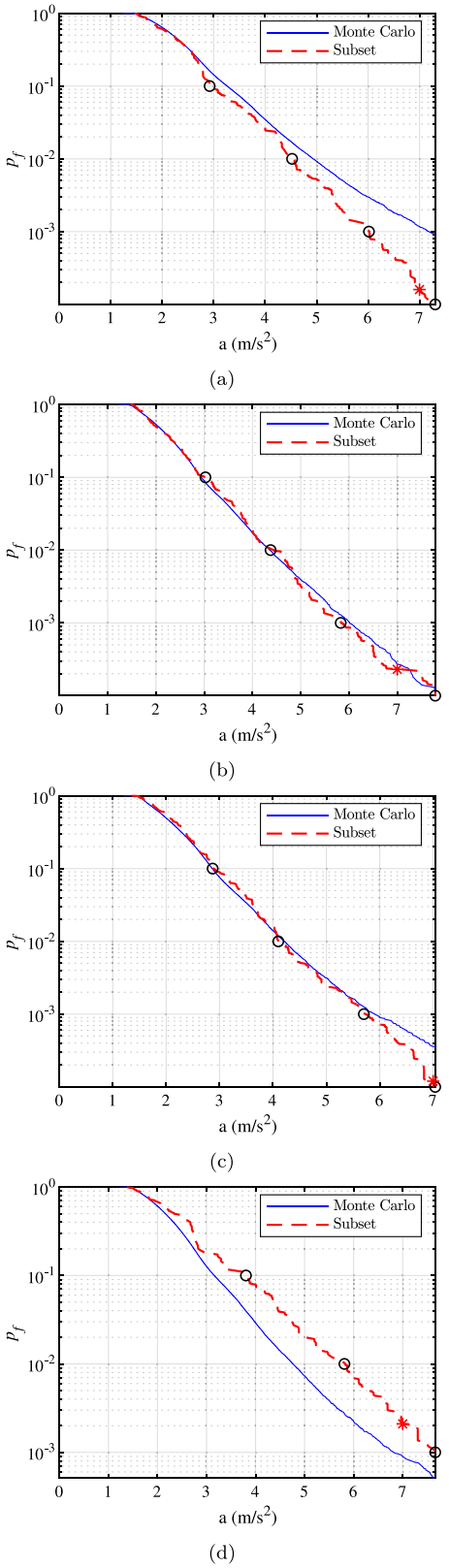

Fig. 13. Complementary CDF of the subset simulations (HSLM-A3, p_0 = 0.1, N = 100) and corresponding Monte Carlo simulations with N = 100000. (a) y_t = 2.0 m/s^2, v_{crit} = 266 km/h; (b) y_t = 2.5 m/s^2, v_{crit} = 264 km/h; (c) y_t = 3.0 m/s^2, v_{crit} = 263 km/h; (d) y_t = 3.5 m/s^2, v_{crit} = 267 km/h.

Table 3
Variation of the intermediate probability p_0 (HSLM-A3, $y_t = 3.0$, $N = 100$).

p_0	0.05	0.1	0.2
time (h)	2:49	1:48	2:37
n_S	2700	2200	3700
v_{crit} (km/h)	264	263	265

Table 4
Variation of the sample size N (HSLM-A3, $y_t = 3.0$, $p_0 = 0.1$).

N	50	100	150	200
time (h)	1:01	1:48	3:26	2:52
n_S	1050	2200	6200	4000
v_{crit} (km/h)	263	263	267	265

5.2. Optimization of the intermediate probability p_0

Using the aforementioned y_t value and a fixed sample size $N = 100$, the optimal intermediate probability is examined by varying p_0 between 0.05, 0.1 and 0.2. As shown in Table 3, adopting an intermediate probability of 0.1 allowed the algorithm to converge in the shortest time and with the smallest total sample size. The effect of using $p_0 = 0.2$ was similar to that of having a high y_t, i.e., given the intermediate probability, the cut-off on the ordered results' list is made at a lower value. This makes it harder for y^* to achieve y_t, which in turn makes for a longer $v = v - 1$ reverse search cycle. As for the lower value, 0.05, the resulting additional computing time would only be justifiable if the target p_f was lower than 10^{-4}.

The comparison of complementary CDFs of subset simulation with the equivalent crude Monte Carlo simulations with $N = 100000$ is shown in Fig. 14. It is noticed that the simulation with $p_0 = 0.2$ corresponds to a larger deviation when compared to the Monte Carlo assessments. Conversely, the same trends are closer for $p_0 = 0.2$, albeit at a higher computational cost.

5.3. Optimization of the sample size N

Regarding the sample size, the comparison of N between 50, 100, 150 and 200 is calculated with fixed $y_t = 3.0$ and $p_f = 0.1$. Unsurprisingly, Table 4 reveals that it takes more time to compute larger sample sizes, while the smallest size, 50, corresponds to the least amount of time and smallest total sample size. However, with an intermediate probability of 0.1, each level of a subset simulation with $N = 50$ provides only 5 elements to generate the samples of the following level. As a result, the number of failed candidate states in the MMA increases, introducing inefficacy when scaling the method by artificially limiting the dispersion of the results.

The verification of the optimization results against Monte Carlo simulations is given in Fig. 15. Observing its complementary CDFs, it is worth noting that there is an increased unevenness for $N = 50$, even if the resulting critical speed is the same as for $N = 100$. The larger sample sizes of $N = 150$ and $N = 200$ lead to similar results while consuming more computation time.

Given that the various applications lead to v_{crit} in close proximity, the final adopted values are $y_t = 3.0$ m/s^2, $p_0 = 0.1$, and $N = 100$.

6. Simulation results

6.1. Calculated critical speeds

The current section represents the application of the first step of the methodology. After setting the optimal factors in the algorithm, the critical speeds on each bridge are calculated for each HSLM-A train model. The individual critical speeds $v_{crit,i}$ are listed in Table 5. The final critical speed values are highlighted in the same table.

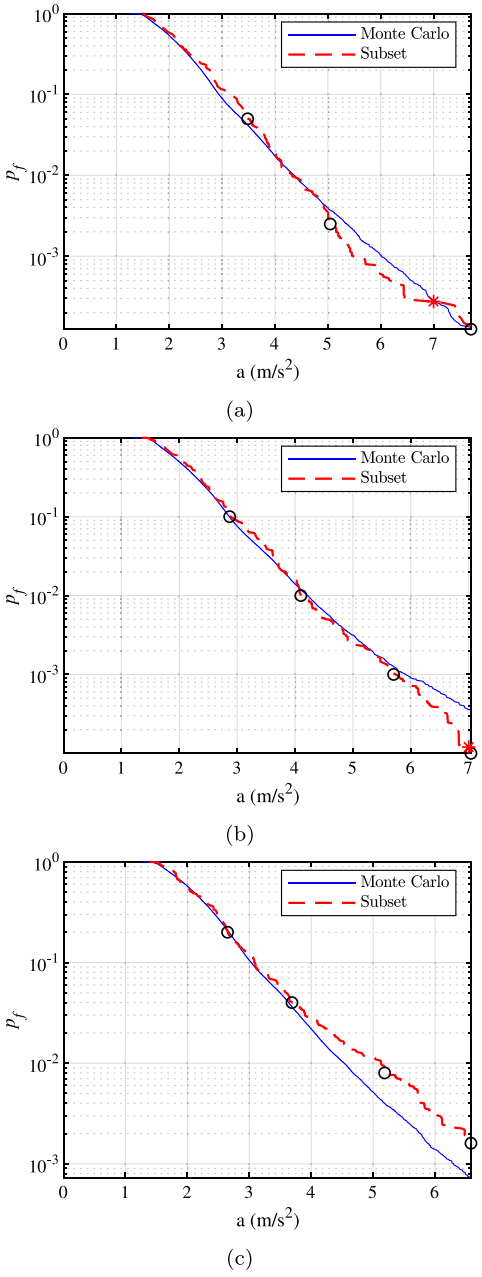

Fig. 14. Complementary CDF of the subset simulations (HSLM-A3, $y_t = 3.0$ m/s^2, $N = 100$) and corresponding Monte Carlo simulations with $N = 100000$. (a) $p_0 = 0.05$, $v_{crit} = 264$ km/h; (b) $p_0 = 0.1$, $v_{crit} = 263$ km/h; (c) $p_0 = 0.2$, $v_{crit} = 265$ km/h.

6.2. Assessment of scenarios for bridge design

The present section showcases the application of the second step of the methodology, where the scenarios for bridge design are defined as two sets of instructions on how to assign values to several random variables. The selection of the variables to be included in the definition of the scenarios is achieved through a sensitivity analysis, where the importance of each variable is assessed with Eq. (3). Here, the study is performed for the Canelas bridge, using the 10 HSLM-A load configurations and a train speed interval from 140 km/h to 420 km/h. The calculated variance values are listed in Table 6. It can be seen that there is a remarkable importance of the variables that control most of the structural mass (thickness and density of both the slab and

Table 5
Critical speeds for each HSLM-A train model.

HSLM	$v_{crit,i}$ (km/h)			
	Canelas bridge	Melga bridge	Cascalheira underpass	Braço do Cortiço underpass
A1	414	N/A	250	244
A2	361	175	269	156
A3	263	173	263	255
A4	274	179	277	146
A5	284	185	284	264
A6	293	192	287	263
A7	298	194	289	244
A8	314	202	301	282
A9	316	205	261	252
A10	325	214	254	255

Table 6
Sensitivity analysis of the relative influence of the variables.

Variable	Variance	
	Y lower envelope	**Y** upper envelope
Reinforced concrete density ρ_C	1.06	1.08
Concrete elasticity modulus E_C	2.63	1.46
Slab thickness t_{slab}	1.56	1.43
Slab width b_{slab}	0.06	0.06
Area of the steel profiles A_S	0.06	0.06
Structural damping ξ	2.29	1.13
Ballast density ρ_b	1.04	1.21
Ballast elasticity modulus E_b	0.02	0.02
Ballast layer height h_b	0.66	1.56
Load distribution angle α	0.02	0.02
Sleeper mass m_s	0.01	0.12
Rail pad stiffness k_p	0.03	0.02
Track shear stiffness k_t	0.20	0.03
Neoprene shear modulus G_n	1.29	0.53

Table 7
Scenarios for bridge design.

Scenario	E_c, ξ	ρ_C, t_{slab}	ρ_b, h_b	G_n
S1	$\mu - 1.64\sigma$	$\mu - 1.64\sigma$	$a + 0.05\,(b-a)$	$a + 0.05\,(b-a)$
S2	$\mu - 1.64\sigma$	$\mu + 1.64\sigma$	$a + 0.95\,(b-a)$	$a + 0.05\,(b-a)$

the ballast layer) and of the concrete stiffness. Structural damping and support stiffness also account for a considerable portion. Due to the clear difference in the results, the variables that score a variance result (from Eq. (3)) greater than 1 are selected for the definition of the design scenarios.

Consequently, the deterministic scenarios S1 and S2 are proposed in Table 7. In accordance with the EN 1991-2 [2], there are two estimates of mass (upper and lower bound), defined by thickness and density (t_{slab}, h_b, ρ_C, ρ_b), combined with a single estimate (lower bound) of stiffness (E_C, G_n) and structural damping (ξ).

Using the definitions of Table 7 and setting the remaining random variables to their mean values, the dynamic design response can be obtained. Fig. 16 represents the response envelopes of the deterministic scenarios for the case study bridges. It is worth noting that these bridges were originally designed in the 1990s for a train speed of 160 km/h, hence the large acceleration values at higher speeds. At the time, the design likely followed standards that did not include dynamic checks with load models similar to the HSLM, possibly relying on static load models affected by amplification factors. The methodology being used in this work may allow for higher permissible deck accelerations, which may in turn enable increased train speeds. Such a study is helpful in addressing the sustainability of existing infrastructure by considering the need to deploy newer, faster, and longer trains to operators' rolling stock rather than replacing existing bridges.

Analyzing the local maxima on the plotted data, it is clear that S1 (with its lower bound estimate of the random variables controlling the structural mass) produces the highest acceleration values, albeit at higher speeds. Conversely, the upper estimates in S2 correspond to lower acceleration peaks, but avoid overestimating the resonant speeds. These observations help to validate the purpose of the scenarios, which corresponds to the Eurocode expects. The design acceleration values a_{Ed} are to be found in these curves at v_{crit}.

Table 8
Design accelerations and safety ratios.

Bridge	a_{Ed} $(\mathrm{m/s^2})$	γ_{bt}
Canelas bridge	4.59	1.52
Melga bridge	5.57	1.26
Cascalheira underpass	5.27	1.33
Braço do Cortiço underpass	5.46	1.28

6.3. Design acceleration and safety ratios

The third and final step of the methodology is performed in this section. Knowing the critical speeds and the envelopes of the design scenarios, the design accelerations a_{Ed} can be found, as illustrated in Fig. 17. The values are given in Table 8, together with the safety ratios, according to Eq. (4).

From the results, it can be observed that a bridge design made with the current Eurocode limit of 3.5 $\mathrm{m/s^2}$ (i.e., with the safety ratio of 2.0) would either limit the maximum allowable train speed or result in heavier, more robust cross-sections. Conversely, the present approach suggests that safety would be ensured up to the calculated critical speeds within the target probability of failure.

7. Conclusion

In this study, the permissible acceleration limit in ballasted track bridges is addressed by defining a design phase acceleration. Two design scenarios are proposed where the design acceleration is found at a critical speed. This speed is assessed using a newly proposed algorithm to overcome the computational challenges associated with low probabilities of failure. The main conclusions of this study can be summarized according to the research gaps identified in Section 1.4:

1. The employment of subset simulation is cost effective when estimating low probabilities of failure. However, it still depends on knowing where to start the search in the speed range. By using an appropriate first-level threshold value, sample size, and intermediate probability, a simple decision-making algorithm can aid in rapidly going through the speed range.
2. The Eurocode EN 1991-2 dictates how stiffness, damping, and mass must be estimated, but does not specify how they are to be achieved. By describing the geometric and material properties of a bridge with basic random variables, it is possible to sample these variables and construct two design scenarios. An expedited sensitivity analysis is sufficient to highlight the most contributing variables;

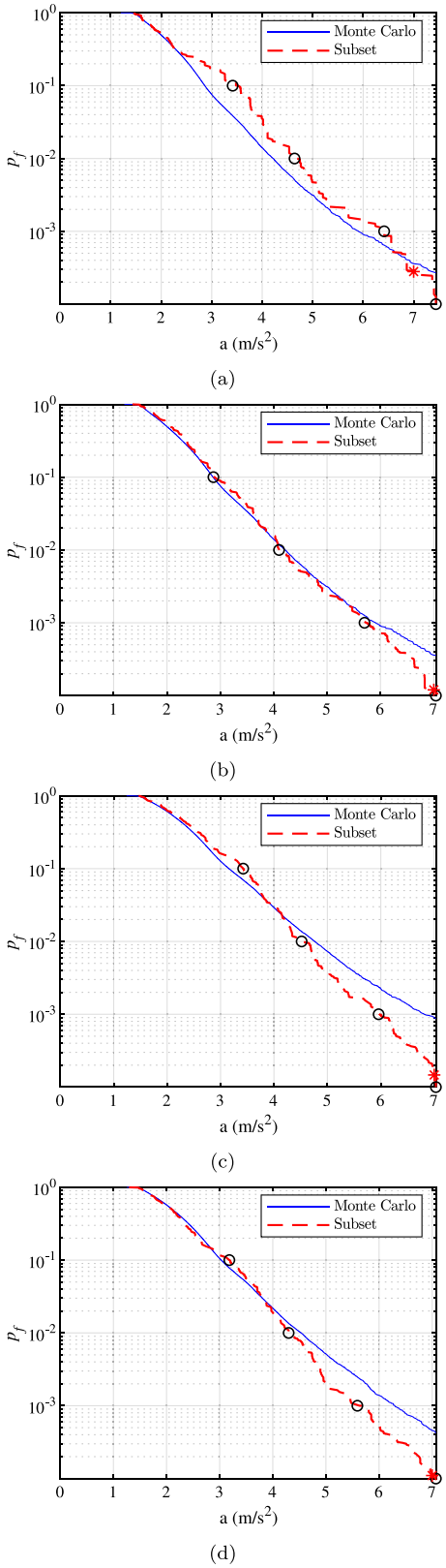

Fig. 15. Complementary CDF of the subset simulations (HSLM-A3, y_t = 3.0 m/s^2, p_0 = 0.1) and corresponding Monte Carlo simulations with N = 100000. (a) N = 50, v_{crit} = 263 km/h; (b) N = 100, v_{crit} = 263 km/h; (c) N = 150, v_{crit} = 267 km/h; (d) N = 200, v_{crit} = 265 km/h.

3. The study of four real ballasted track structures has revealed that a ballasted track bridge can be designed so that its deck can experience an acceleration value greater than 3.5 m/s^2 without being associated with a probability of failure greater than 10^{-4}. Considering that the experimentally assessed acceleration limit is kept at 7 m/s^2, this means that the safety ratio, computed as the ratio between that physical limit and the allowable acceleration, can be set lower than 2.0.

Considering that the calculated design acceleration values are greater than 3.5 m/s^2 (or, in other words, that the associated safety ratios are less than 2.0), it can be concluded that the normative limits are, at least, conservative. Therefore, a revised version of the EN 1990 could allow higher permissible deck acceleration values for ballasted railway bridges. Nonetheless, this study is performed on existing bridges that are currently in operation. Since the second generation of Eurocodes the EN 1990 will be separated into two parts [43] (one focusing new structures and the other for existing structures), future revisions of Eurocodes could consider different design allowance for new and existing bridges, balancing safety with sustainability objectives.

This study represents a first step toward assessing the conservativeness of the current Eurocode safety ratio for deck acceleration. While the findings suggest that the normative limit may be conservative, future research work should extend the methodology to a broader range of bridge types and address systematic modeling uncertainties through experimental calibration and model validation.

CRediT authorship contribution statement

Gonçalo Ferreira: Writing – original draft, Visualization, Investigation, Formal analysis. **Pedro Montenegro:** Writing – review & editing, Methodology, Conceptualization. **Christoph Adam:** Writing – review & editing, Validation, Conceptualization. **António Abel Henriques:** Writing – review & editing, Supervision, Methodology. **Rui Calçada:** Supervision, Resources, Conceptualization.

Declaration of competing interest

The authors declare that they have no known competing financial interests or personal relationships that could have appeared to influence the work reported in this paper.

Acknowledgments

The authors would like to acknowledge Infraestruturas de Portugal for providing technical drawings of the bridges. The authors would like to acknowledge the financial support of :

• “InBridge4EU - Enhanced Interfaces and train categories for dynamic compatibility assessment of European railway bridges” project funded by the Europe’s Rail Joint Undertaking under Horizon Europe Research And Innovation Programme under grant agreement No. 101121765 (HORIZON-ER-JU-2022-ExplR-02). Views and opinions expressed are however those of the author(s) only and do not necessarily reflect those of the European Union or Europe’s Rail Joint Undertaking. Neither the European Union nor the granting authority can be held responsible for them;

• Portuguese Foundation for Science and Technology (FCT) through the PhD scholarship PD/BD/143007/2018;

• Base Funding - UIDB/04708/2020 of the CONSTRUCT - Instituto de I&D em Estruturas e Construções - funded by national funds through the FCT/MCTES (PIDDAC).

Data availability

Data will be made available on request.

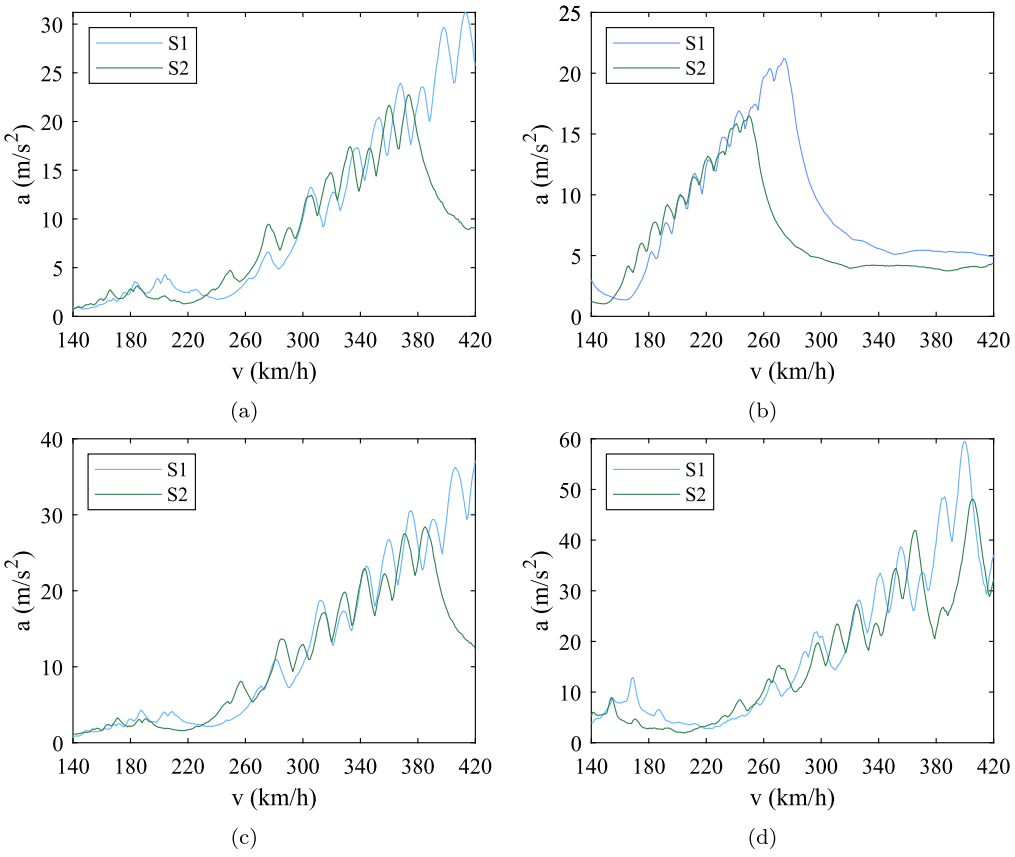

Fig. 16. Design scenario response envelopes. (a) Canelas bridge; (b) Melga bridge; (c) Cascalheira underpass; (d) Braço do Cortiço underpass.

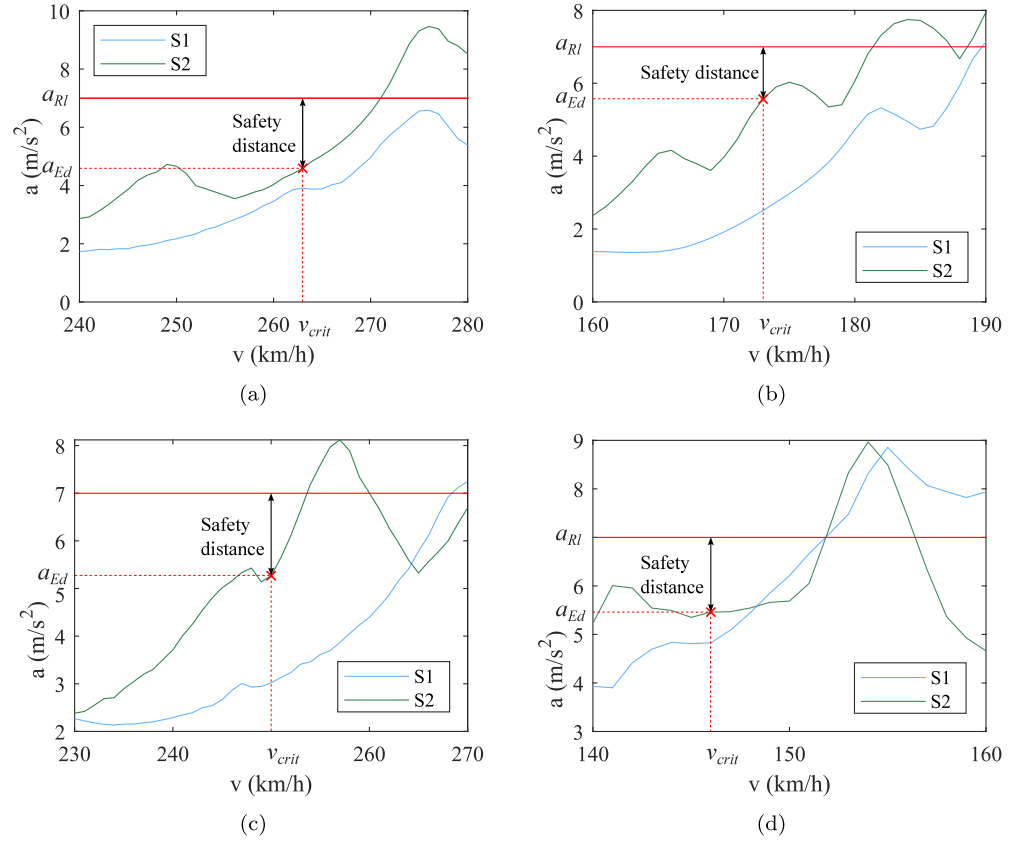

Fig. 17. Critical speeds and design phase accelerations. (a) Canelas bridge; (b) Melga bridge; (c) Cascalheira underpass; (d) Braço do Cortiço underpass.

References

[1] CEN. Eurocode - Basis of structural and geotechnical design. EN 1990, Brussels: Commité European de Normalisation (CEN); 2023.

[2] CEN. Eurocode 1 - Actions on structures - Part 2: Traffic loads on bridges and other civil engineering works. EN 1991–2, Brussels: Commité European de Normalisation (CEN); 2023.

[3] ERRI D 214/RP 9. Rail bridges for speeds > 200 Km/h. Final Report, Utrecht: European Rail Research Institute; 1999.

[4] Zacher M, Baeßler M. Dynamic behaviour of ballast on railway bridges. In: Dynamics of high–speed railway bridges. selected and revised papers from the advanced course on 'dynamics of high–speed railway bridges', porto, Portugal, 20–23 September 2005. CRC Press; 2008, p. 125–42.

[5] European Union Agency for Railways (ERA). ERA1193-TD-01-2022 - ERA technical note on work needed for closing TSI open points on bridge dynamics. 2022, URL https://rail-research.europa.eu:443/about-europes-rail/europes-rail-reference-documents/additional-technical-material/.

[6] European Comission. Consolidated text: Commission Decision of 30 May 2002 concerning the technical specification for interoperability relating to the infrastructure subsystem of the trans-European high-speed rail system referred to in Article 6(1) of Council Directive 96/48/EC (notified under document number C(2002) 1948) (Text with EEA relevance) (2002/732/EC). 2002, p. 143, URL https://eur-lex.europa.eu/eli/dec/2002/732/2002-09-12.

[7] Heiland T, Hägle M, Triantafyllidis T, Stempniewski L, Stark A. Stiffness contributions of ballast in the context of dynamic analysis of short span railway bridges. Constr Build Mater 2022;360:129536. http://dx.doi.org/10.1016/j.conbuildmat.2022.129536, URL https://www.sciencedirect.com/science/article/pii/S0950061822031920.

[8] Stollwitzer A, Bettinelli L, Fink J. Vertical track-bridge interaction in railway bridges with ballast superstructure: Experimental analysis of dynamic stiffness and damping behavior. Int J Struct Stab Dyn 2024. http://dx.doi.org/10.1142/S0219455425400085.

[9] Menezes J. Modelling of the dynamic behaviour of ballast on railway bridges (Master's thesis), Porto, Portugal: Faculdade de Engenharia da Universidade do Porto; 2024, URL https://repositorio-aberto.up.pt/handle/10216/162090.

[10] Hou B, Wang D, Wang B, Chen X, Pombo J. Vibration Reduction in Ballasted Track Using Ballast Mat: Numerical and Experimental Evaluation by Wheelset Drop Test. Appl Sci 2022;12(4):1844. http://dx.doi.org/10.3390/app12041844, URL https://www.mdpi.com/2076-3417/12/4/1844.

[11] Zhai WM, Wang KY, Lin JH. Modelling and experiment of railway ballast vibrations. J Sound Vib 2004;270(4):673–83. http://dx.doi.org/10.1016/S0022-460X(03)00186-X, URL https://www.sciencedirect.com/science/article/pii/S0022460X0300186X.

[12] Salcher P, Pradlwarter H, Adam C. Reliability assessment of railway bridges subjected to high-speed trains considering the effects of seasonal temperature changes. Eng Struct 2016;126:712–24. http://dx.doi.org/10.1016/j.engstruct.2016.08.017, URL https://www.sciencedirect.com/science/article/pii/S0141029616304175.

[13] Rocha JM. Probabilistic methodologies for the safety assessment of short span railway bridges for high-speed traffic (Ph.D. thesis), Porto, Portugal: Faculdade de Engenharia da Universidade do Porto; 2015, URL https://repositorio-aberto.up.pt/handle/10216/83809.

[14] Salcher P, Pradlwarter H, Adam C. Reliability of high-speed railway bridges with respect to uncertain characteristics. In: 9th European conference on structural dynamics. Porto, Portugal; 2014.

[15] Mao J, Yu Z, Xiao Y, Jin C, Bai Y. Random dynamic analysis of a train-bridge coupled system involving random system parameters based on probability density evolution method. Probabilistic Eng Mech 2016;46:48–61. http://dx.doi.org/10.1016/j.probengmech.2016.08.003, URL https://www.sciencedirect.com/science/article/pii/S0266892016300972.

[16] Xin L, Li X, Zhu Y, Liu M. Uncertainty and sensitivity analysis for train-ballasted track–bridge system. Veh Syst Dyn 2020;58(3):453–71. http://dx.doi.org/10.1080/00423114.2019.1584678.

[17] Xu Z, Dai G, Chen YF, Rao H, Huang Z. Extreme response analysis of train-track-bridge-wind interaction system based on in-situ monitoring wind data. Struct Saf 2023;100:102288. http://dx.doi.org/10.1016/j.strusafe.2022.102288, URL https://www.sciencedirect.com/science/article/pii/S0167473022000959.

[18] Park J, Towashiraporn P. Rapid seismic damage assessment of railway bridges using the response-surface statistical model. Struct Saf 2014;47:1–12. http://dx.doi.org/10.1016/j.strusafe.2013.10.001, URL https://www.sciencedirect.com/science/article/pii/S0167473013000787.

[19] Rocha JM, Henriques AA, Calçada R. Probabilistic assessment of the train running safety on a short-span high-speed railway bridge. Struct Infrastruct Eng 2016;12(1):78–92. http://dx.doi.org/10.1080/15732479.2014.995106.

[20] Allahvirdizadeh R, Andersson A, Karoumi R. Reliability assessment of the dynamic behavior of high-speed railway bridges using first order reliability method. In: 11th international conference on structural dynamics, vol. 2, Athens, Greece; 2020, p. 3438–50.

[21] Grigoriou V, Brühwiler E. Monitoring-based safety verification at the Ultimate Limit State of fracture of the RC slab of a short span railway underpass. Struct Saf 2016;60:16–27. http://dx.doi.org/10.1016/j.strusafe.2016.01.002, URL https://www.sciencedirect.com/science/article/pii/S0167473016000138.

[22] Hirzinger B, Adam C, Salcher P, Oberguggenberger M. On the optimal strategy of stochastic-based reliability assessment of railway bridges for high-speed trains. Meccanica 2019;54(9):1385–402. http://dx.doi.org/10.1007/s11012-019-00999-0.

[23] Salcher P, Adam C. Estimating Exceedance Probabilities of Railway Bridge Vibrations in the Presence of Random Rail Irregularities. Int J Struct Stab Dyn 2020;20(13):2041005. http://dx.doi.org/10.1142/S0219455420410059, URL https://www.worldscientific.com/doi/abs/10.1142/S0219455420410059.

[24] Hirzinger B, Adam C, Oberguggenberger M, Salcher P. Approaches for predicting the probability of failure of bridges subjected to high-speed trains. Probabilistic Eng Mech 2020;59:103021. http://dx.doi.org/10.1016/j.probengmech.2020.103021, URL https://www.sciencedirect.com/science/article/pii/S0266892020300060.

[25] JCSS. Probabilistic model code. JCSS-OSTL/DIA/VROU -10-11-2000, Joint Commitee on Structural Safety (JCSS); 2001, URL https://www.jcss-lc.org/jcss-probabilistic-model-code/.

[26] Bjerager P. Methods for structural reliability computations. In: Casciati F, Roberts JB, editors. Reliability problems: general principles and applications in mechanics of solids and structures. International centre for mechanical sciences, Springer; 1991, p. 89–135. http://dx.doi.org/10.1007/978-3-7091-2616-5_3.

[27] Au S-K, Beck JL. Estimation of small failure probabilities in high dimensions by subset simulation. Probabilistic Eng Mech 2001;16(4):263–77. http://dx.doi.org/10.1016/S0266-8920(01)00019-4, URL https://www.sciencedirect.com/science/article/pii/S0266892001000194.

[28] Zuev KM. Subset simulation method for rare event estimation: An introduction. In: Beer M, Kougioumtzoglou IA, Patelli E, Au IS-K, editors. Encyclopedia of earthquake engineering. Springer; 2013, p. 1–25. http://dx.doi.org/10.1007/978-3-642-36197-5_165-1.

[29] ANSYS®. Release 19.2. ANSYS Inc.; 2018.

[30] MATLAB®. Academic Research. MathWorks Inc.; 2018.

[31] Ferreira G, Montenegro P, Pinto J, Henriques A, Calçada R. A discussion about the limitations of the Eurocode's high-speed load model for railway bridges. Railw Eng Sci 2024;32(2):211–28. http://dx.doi.org/10.1007/s40534-023-00321-5.

[32] Horas CCdS. Comportamento Dinâmico de Pontes Com Tabuleiro Pré-Fabricado Em Vias de Alta Velocidade (Master's thesis), Porto, Portugal: Faculdade de Engenharia da Universidade do Porto; 2011, URL https://repositorio-aberto.up.pt/handle/10216/66380.

[33] Uribe F. Monte Carlo and subset simulation example. 2016, URL https://www.mathworks.com/matlabcentral/fileexchange/57947-monte-carlo-and-subset-simulation-example.

[34] Vorwagner A, Kwapisz M, Flesch R, Kohl AM, Firus A, Vospernig M, Arana Villafán T. FEM based approach for development of a new high-speed load model for railway bridges. 2021, p. 1614–22. http://dx.doi.org/10.2749/ghent.2021.1614, URL https://structurae.net/de/fachliteratur/tagungsbeitrag/fem-based-approach-for-development-of-a-new-high-speed-load-model-for-railway-bridges.

[35] Allahvirdizadeh R, Andersson A, Karoumi R. Partial safety factor calibration using surrogate models: An application for running safety of ballasted high-speed railway bridges. Probabilistic Eng Mech 2024;75:103569. http://dx.doi.org/10.1016/j.probengmech.2023.103569, URL https://www.sciencedirect.com/science/article/pii/S0266892023001583.

[36] Fortunato EMC. Renovação de Plataformas Ferroviárias : Estudos Relativos à Capacidade de Carga (Ph.D. thesis), Porto, Portugal: Faculty of Engineering of the University of Porto, Porto, Portugal; 2005, URL https://repositorio-aberto.up.pt/handle/10216/11441.

[37] UIC. Best practice guide for optimum track geometry durability. Technical Report, Paris: Union Internationale des Chemins de fer; 2008.

[38] Salcher P. Reliability assessment of railway bridges designed for high-speed traffic: Modeling strategies and stochastic simulation (Ph.D. thesis), Innsbruck, Austria: University of Innsbruck; 2015.

[39] Manterola J. Puentes: apuntes para su diseño, cálculo y construcción. Madrid, Spain: Colegio de Ingenieros de Caminos, Canales y Puertos; 2006.

[40] Bonifácio C, Ribeiro D, Calçada R, Delgado R. Calibration and validation of the numerical model of a short-span railway bridge based on dynamic tests. In: Proceedings of the 9th international conference on structural dynamics. 2014.

[41] Pimentel R, Barbosa C, Costa N, Ribeiro D, Ferreira LA, Araújo FM, Calçada R. Characterization of railway traffic and its effects on a short span bridge by using a hybrid fibre optic/electrical measurement system. In: Third European workshop on optical fibre sensors. International Society for Optics and Photonics; 2007, http://dx.doi.org/10.1117/12.738786, URL https://www.spiedigitallibrary.org/conference-proceedings-of-spie/6619/66193Y/Characterization-of-railway-traffic-and-its-effects-on-a-short/10.1117/12.738786.short.

[42] Silva A, Ribeiro D, Montenegro P, Ferreira G, Andersson A, Zangeneh A, Karoumi R, Calçada R. New contributions for damping assessment on filler-beam railway bridges framed on In2Track EU projects. Appl Sci (Switzerland) 2023;13(4). http://dx.doi.org/10.3390/app13042636.

[43] Formichi P. EN 1990: Basis of structural design. In: EUROCODE conference. 2023, URL https://www.dibt.de/en/news/events/date-detail-page/termin/eurocode-conference-2023-recording-and-presentations.